International Journal of Multiphase Flow 36 (2010) 672–681

Contents lists available at ScienceDirect

International Journal of Multiphase Flow

journal homepage: www.elsevier.com/locate/ijmulflow

An icing physics study by using lifetime-based molecular tagging thermometry technique

Hui Hu *, Zheyan Jin [1]

Department of Aerospace Engineering, Iowa State University, Ames, IA 50011, USA

ARTICLE INFO

Article history:
Received 6 October 2009
Received in revised form 18 January 2010
Accepted 12 April 2010
Available online 18 April 2010

Keywords:
Molecular tagging thermometry
Icing physics of water droplets
Solidification process
Micro scale heat transfer
Wind turbine icing

ABSTRACT

An experimental investigation was conducted to quantify the unsteady heat transfer and phase changing process within small icing water droplets in order to elucidate underlying physics to improve our understanding of the important micro-physical process of icing phenomena. A novel, lifetime-based molecular tagging thermometry (MTT) technique was developed and implemented to achieve temporally-and-spatially resolved temperature distribution measurements to reveal the time evolution of the unsteady heat transfer and dynamic phase changing process within micro-sized water droplets in the course of icing process. It was found that, after a water droplet impinged onto a frozen cold surface, the liquid water at the bottom of the droplet would be frozen and turned to solid ice rapidly, while the upper portion of the droplet was still in liquid state. As the time goes by, the interface between the liquid phase water and solid phase ice was found to move upward continuously with more and more liquid water within the droplet turned to solid ice. Interestingly, the averaged temperature of the remaining liquid water within the small icing droplet was found to increase, rather than decrease, continuously in the course of icing process. The temperature increase of the remaining liquid water is believed to be due to the heat release of the latent heat during solidification process. The volume expansion of the water droplet during the icing process was found to be mainly upward to cause droplet height growth rather than radial to enlarge the contact area of the droplet on the test plate. As a result, the spherical-cap-shaped water droplet was found to turn to a prolate-spheroid-shaped ice crystal with cusp-like top at the end of the icing process. The required freezing time for the water droplets to turn to ice crystals completely was found to depend on the surface temperature of the test plate strongly, which would decrease exponentially as the surface temperature of the frozen cold test plate decreases.

© 2010 Elsevier Ltd. All rights reserved.

1. Introduction

Wind energy is one of the cleanest renewable power sources in the world today. The US Department of Energy has challenged the nation to produce 20% of its total power from wind by 2030. According to *American Wind Energy Association* (AWEA), the majority of wind energy potential available in US are in the oceans off the eastern and western seaboard and in the northern states such as North Dakota, Kansas, South Dakota, Montana, Nebraska, Wyoming, Minnesota, and Iowa, where wind turbines are subjected to the problems caused by cold climate conditions. Wind turbine icing represents the most significant threat to the integrity of wind turbines in cold weather. It has been found that ice accretion on turbine blades would decrease power production of the wind turbines significantly (Laakso and Peltola, 2005). Ice accretion and irregular shedding during wind turbine operation would lead to load imbalances as well as excessive turbine vibration, often causing the wind turbine to shut off (Dalili et al., 2009). Icing can also affect the tower structures by increasing stresses. This can lead to structural failures, especially when coupled to strong wind loads (Jasinski et al., 1998). Icing was also found to affect the reliability of anemometers, thereby, leading to inaccurate wind speed measurements and resulting in resource estimation errors (Homola et al., 2006). Icing issues can also directly impact personnel safety due to falling and projected large ice chunks (Seifert et al., 2003).

Due to lack of knowledge, current ice prediction tools and ice protection system designs for wind turbine applications make use of simple classical models which ignore many details of the important micro-physical processes that are responsible for the ice formation and accretion on wind turbines (Hansman and Turnock, 1989; Jasinski et al., 1998). Advancing the technology for safe and efficient wind turbine operation in atmospheric icing conditions requires a better understanding of the important micro-physical phenomena pertinent to wind turbine icing phenomena. While several studies have been carried out recently to simulate ice

* Corresponding author.
E-mail address: huhui@iastate.edu (H. Hu).
[1] Present address: School of Aerospace Engineering and Mechanics, Tongji University, China.

0301-9322/$ - see front matter © 2010 Elsevier Ltd. All rights reserved.
doi:10.1016/j.ijmultiphaseflow.2010.04.001

accretion on turbine blades through icing wind tunnel testing (Hochart et al., 2008) or using "artificial" iced profiles with various types and amounts of ice accretion to investigate the aerodynamic performance and power output for iced blades (Tammelin et al., 1998), very few fundamental studies can be found in literature to elucidate underlying physics associated with wind turbine icing phenomena. In order to elucidate the underlying physics associated with the important micro-physical processes, fundamental icing physics studies capable of providing detailed information to quantify important ice formation and ice-growth physical processes such as droplet dynamics, unsteady heat transfer process within water droplets or ice crystals, and phase changing process of water droplets and water film flows over smooth/rough surfaces, are highly desirable.

In the present study, an experimental investigation is conducted to quantify the unsteady heat transfer and phase changing process within small icing water droplets in order to elucidate underlying physics to improve our understanding of the important micro-physical process pertinent to wind turbine icing phenomena. A novel, lifetime-based molecular tagging thermometry (MTT) technique is developed to achieve temporally-and-spatially resolved temperature distribution measurements to reveal the time evolution of the unsteady heat transfer and dynamic phase changing process within small icing water droplets in the course of icing process, which is pertinent to the ice formation and accretion process as water droplets impinge onto frozen cold wind turbine blades. The underlying physics of the micro-physical processes that are responsible for the icing formation and accretion within small icing water droplets is elucidated in great detail. To the best knowledge of the authors, this is the first effort of its nature. The new findings derived from the icing physics studies as the one reported here will lead to a better understanding of the important micro-physical processes, which could be used to improve current icing accretion models for more accurate prediction of ice formation and ice accretion on wind turbine blades as well as development of effective anti-/de-icing strategies tailored for wind turbine icing mitigation and icing protection.

The Lifetime-based MTT technique used in the present study can be considered as an extension of the Molecular Tagging Velocimetry and Thermometry (MTV&T) technique developed by Hu and Koochesfahani (2006). While all the previous studies by using the lifetime–based MTT technique were conducted in single-phase flows (Hu and Koochesfahani, 2003, 2006; Hu and Huang, 2009), the work presented here will deal with a multiphase flow system involving a harsh environment of low temperature and phase changing process. In the sections that follow, the technical basis of the lifetime-based MTT will be described briefly along with the related properties of the phosphorescent tracer molecules used for the lifetime-based MTT measurements. Then, the application of the lifetime-based MTT technique to quantify the time evolution of the unsteady heat transfer and phase changing process within small icing water droplets in the course of icing process will be given to elucidate underlying physics to improve our understanding of the important micro-physical phenomena pertinent to wind turbine icing phenomena.

2. Lifetime-based MTT technique

It is well known that both *fluorescence* and *phosphorescence* are molecular photoluminescence phenomena. Compared with *fluorescence*, which typically has a lifetime on the of order nanoseconds, *phosphorescence* can last as long as microseconds, even minutes. Since emission intensity is a function of the temperature for some substances, both *fluorescence* and *phosphorescence* of tracer molecules may be used for temperature measurements. *Laser-induced fluorescence* (LIF) techniques have been widely used for temperature measurements of liquid droplets for combustion applications (Lu and Melton, 2000; Wolff et al., 2007). Harris et al. (1996) used a LIF-based technique to conduct quantitative measurements of internal circulation in droplets. *Laser-induced phosphorescence* (LIP) techniques have also been suggested recently to conduct temperature measurements of "in-flight" or levitated liquid droplets (Omrane et al., 2004a,b). Compared with LIF techniques, the relatively long lifetime of LIP could be used to prevent interference from scattered/reflected light and any fluorescence from other substances (such as from solid surfaces) that are present in the measurement area, by simply putting a small time delay between the laser excitation pulse and the starting time for phosphorescence image acquisitions. Furthermore, LIP was found to be much more sensitive to temperature variation compared with LIF (Omrane et al., 2004a,b), which is favorable for the accurate measurements of small temperature differences within small liquid droplets. The lifetime-based MTT technique used in the present study is a LIP-based technique.

The technical basis of the proposed lifetime-based MTT measurements is given briefly at here. According to quantum theory (Pringsheim, 1949), the intensity of a first-order photoluminescence process (either *fluorescence* or *phosphorescence*) decays exponentially. As described in Hu et al. (2006), for a diluted solution and unsaturated laser excitation, the collected phosphorescence signal (S) by using a gated imaging detector with integration starting at a delay time t_o after the laser pulse and a gate period of δt can be given by:

$$S = AI_iC\varepsilon\Phi_p\left(1 - e^{-\delta t/\tau}\right)e^{-t_o/\tau} \tag{1}$$

where A is a parameter representing the detection collection efficiency, I_i is the local incident laser intensity, C is the concentration of the phosphorescent dye (the tagged molecular tracer), ε is the absorption coefficient, and ϕ_p is the phosphorescence quantum efficiency. The emission lifetime τ refers to the time at which the intensity drops to 37% (i.e., $1/e$) of the initial intensity. For an excited state, the deactivation process may involve both radiative and non-radiactive pathways. The lifetime of the photoluminescence process, τ, is determined by the sum of all the deactivation rates: $\tau^{-1} = k_r + k_{nr}$, where k_r and k_{nr} are the radiative and non-radiative rate constants, respectively. According to photoluminescence kinetics (Ferraudi, 1988), these rate constants are, in general, temperature-dependant. The temperature dependence of the phosphorescence lifetime is the basis of the present lifetime-based MTT technique.

It is well known that the absorption coefficient ε, quantum yield ϕ_p, and the emission lifetime τ are temperature dependent in general, resulting in a temperature-dependent phosphorescence signal (S). Thus, in principle, the collected phosphorescence signal (S) may be used to measure fluid temperature if the incident laser intensity and the concentration of the phosphorescent dye remain constant (or are known) in the region of interest. It should be noted that the collected phosphorescence signal (S) is also the function of incident laser intensity (I_i) and the concentration of the phosphorescent dye (C). Therefore, the spatial and temporal variations of the incident laser intensity and the non-uniformity of the phosphorescent dye (such as due to photobleaching or expulsion of the dye molecular from the liquid during icing process) in the region of interest would have to be corrected separately in order to derive quantitative temperature data from the acquired phosphorescence images. In practice, however, it is very difficult, if not impossible, to ensure a non-varying incident laser intensity distribution, especially for unsteady thermal phenomena with varying index of refraction. This may cause significant errors in the temperature measurements. To overcome this problem, Hu and Koochesfahani (2003)

developed a lifetime-based thermometry to eliminate the effects of incident laser intensity and concentration of phosphorescent dye on temperature measurements.

The lifetime-based thermometry works as follows: As illustrated in Fig. 1, laser-induced phosphorescence emission is interrogated at two successive times after the same laser excitation pulse. The first image is detected at the time $t = t_o$ after laser excitation for a gate period δt to accumulate the phosphorescence intensity S_1, while the second image is detected at the time $t = t_o + \Delta t$ for the same gate period to accumulate the phosphorescence intensity S_2. It is easily shown (Hu and Koochesfahani, 2006), using Eq. (1), that the ratio of these two phosphorescence signals (R) is given by:

$$R = S_2/S_1 = e^{-\Delta t/\tau} \tag{2}$$

In other words, the intensity ratio of the two successive phosphorescence images (R) is only a funtion of the phosphorescence lifetime τ and the time delay Δt between the image pair, which is a controllable parameter. This ratiometric approach eliminates the effects of any temporal and spatial variations in the incident laser intensity (due to pulse-to-pulse laser energy variations) and non-uniformity of the dye concentration (e.g. due to photobleaching or expulsion of the molecular tracers during icing process). For a given molecular tracer and fixed Δt value, Eq. (2) defines a unique relation between phosphorescence intensity ratio (R) and fluid temperature T, which can be used for thermometry as long as the temperature dependence of phosphorescence lifetime is known.

The phosphorescent molecular tracer used for the present study is phosphorescent triplex (1-BrNp·Mβ-CD·ROH). The phosphorescent triplex (1-BrNp·Mβ-CD·ROH) is actually the mixture compound of three different chemicals, which are lumophore (indicated collectively by 1-BrNp), maltosyl-β-cyclodextrin (indicated collectively by Mβ-CD) and alcohols (indicated collectively by ROH). Further information about the chemical and photoluminescence properties of the phosphorescent triplex (1-BrNp·Mβ-CD·ROH) is available at Hartmann et al. (1996) and Koochesfahani and Nocera (2007). In the present study, we used a concentration of 2×10^{-4} M for Mβ-CD, a saturated (approximately 1×10^{-5} M) solution of 1-BrNp and a concentration of 0.06 M for the alcohol (ROH), as suggested by Gendrich et al. (1997).

Upon the pulsed excitation of a UV laser (quadrupled wavelength of Nd:YAG laser at 266 nm for the present study), the phosphorescence lifetime of the phosphorescent triplex (1-BrNp·Mβ-CD·ROH) molecules in an aqueous solution was found to change significantly with temperature. Fig. 2 shows the measured phosphorescence lifetimes of 1-BrNp·Mβ-CD·ROH molecules as a function of temperature, which were obtained though a calibration experiment similar as those described in Hu and Koochesfahani (2006). It can be seen clearly that phosphorescence lifetime of 1-BrNp·Mβ-CD·ROH molecules varies significantly with increasing temperature, decreasing from about 7.2 ms to 1.1 ms as the temperature changes from 1.0 °C to 40.0 °C. The relative temperature sensitivity of the phosphorescence lifetime is about 3.6% per degree Celsius, which is much higher than those of fluorescent dyes. For comparison, the temperature sensitivity of Rhodamine B widely used for LIF-based thermometry is less than 2.0% per degree Celsius (Coppeta and Rogers, 1998; Hu et al., 2006).

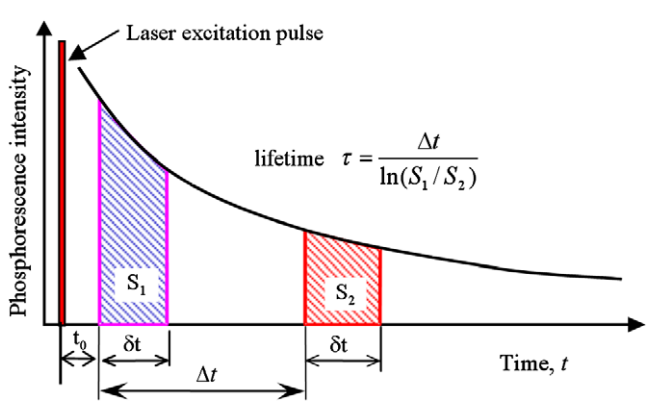

Fig. 1. Timing chart of lifetime-based MTT technique.

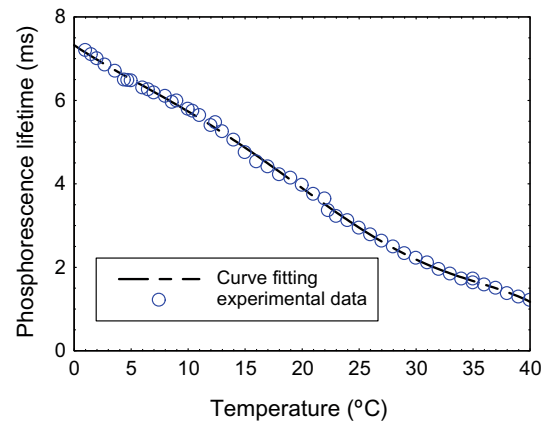

Fig. 2. Phosphorescence lifetime versus temperature.

3. Experimental setup

Fig. 3 shows the schematic of the experimental setup used in the present study to implement the lifetime-based MTT technique to quantify unsteady heat transfer and phase changing process within small icing water droplets to elucidate underlying physics of microphysical process of icing phenomena. A syringe with a sharp needle was used to generate micro-sized water droplets (about 400 μm in radius and 250 μm in height) to impinge onto a test plate to simulate the processes of small water droplets impinging onto a wind turbine blade. The temperature of the test plate, which was monitored by using a thermocouple, was kept constant at a pre-selected low temperature level by using a Water Bath Circulator (Neslab RTE-211). Fig. 4 shows the measured temperature profiles above the test plate when the wall temperature of the test plate was set to $T_W = 5.0$ °C and $T_W = -2.0$ °C. The small water droplets with initial temperature of 20.5 °C (room temperature) would be convectively cooled after they impinged onto the cold test plate. Phase changing process would occur inside the small water droplets when the temperature of the test plate was set to below freezing. A laser sheet (~200 μm in thickness) from a pulsed Nd:YAG laser at a quadrupled wavelength of 266 nm was used to tag the premixed 1-BrNp·Mβ-CD·ROH molecules along the middle plane of the small water droplets. A 12-bit gated intensified CCD camera (PCO Di-Cam-Pro, Cooke Corporation) with a fast decay phosphor (P46) was used to capture the phosphorescence emission. A 10× microscopic objective (Mitsutoyo infinity-corrected, NA = 0.28, depth of field = 3.5 μm) was mounted in the front of the camera. The camera was operated in the dual-frame mode, where two full frame images of phosphorescence were acquired in a quick succession after the same laser excitation pulse. The camera and the pulsed Nd:YAG laser were connected to a workstation via a digital delay generator (BNC 555 Digital Delay-Pulse Generator), which controlled the timing of the laser illumination and the image acquisition. For the lifetime-based MTT measurements in the present study, the first phosphorescence image was acquired at 0.5 ms after the laser excitation pulse and the second image at 3.5 ms after the same laser

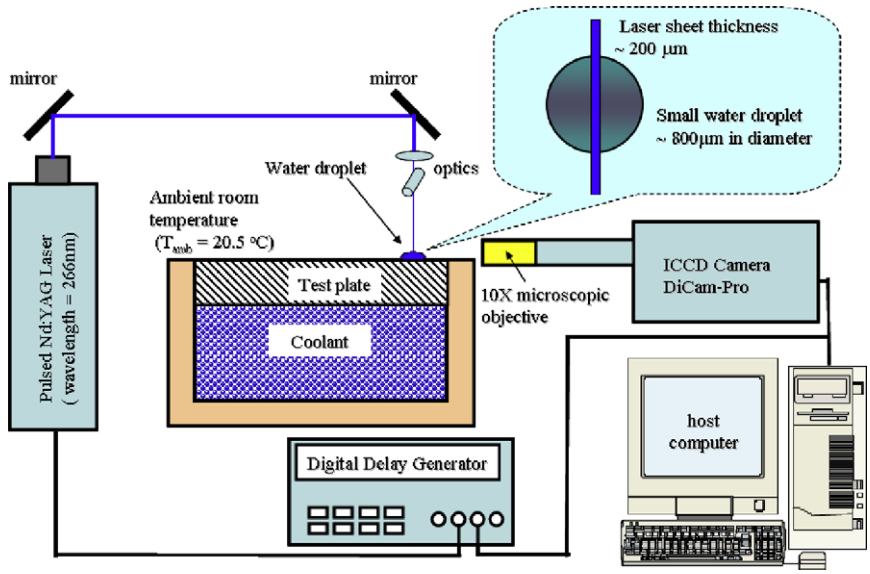

Fig. 3. Experimental setup.

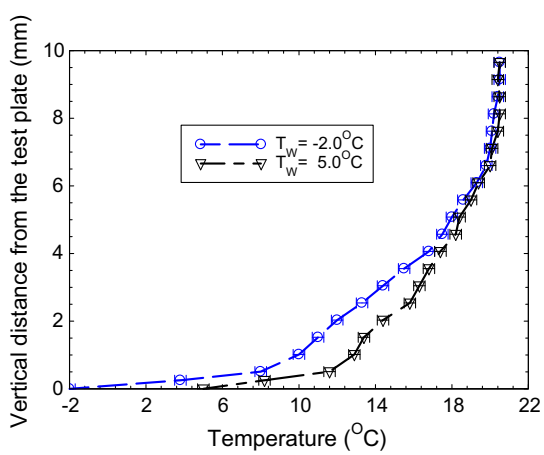

Fig. 4. Measured temperature profiles above the test plate when the surface temperature of the test plate was set to T_W = 5.0 °C and T_W = −2.0 °C.

pulse with the same exposure time of 1.5 ms for the two image acquisitions. It is noted that, since low concentration of the phosphorescent triplex 1-BrNp·Mβ-CD·ROH was used for the present study, the effects of the molecular tracers on the physical properties of water are believed to be negligible. During the experiments, the energy level of the pulse laser used to tag the molecular tracers within small water droplets was below 1.0 mJ/pulse. The repetition rate of the pulsed excitation was 2 Hz. The energy deposited by the excitation laser into the small water droplet was very small, and the temperature rise of the droplets due to the energy deposition of the excitation laser was estimated to be less than 0.1 °C. Further details about the experimental setup and procedures to implement the lifetime-based MTT technique to quantify unsteady heat transfer and phase changing process within small icing water droplets are given in Jin (2008).

4. On the spatial resolution and accuracy of the lifetime-based MTT measurements

As described in Hu and Koochesfahani (2006), like most measurement techniques, the lifetime-based MTT technique used in the present study does not give information at a 'point'. Rather, it provides the spatially-averaged temperature of a molecularly tagged region. Similar to Particle Image Velocimetry (PIV) measurements, the effective spatial resolution of the MTT measurement is given by the sum of the source phosphorescence images leading to noise in the estimated lifetime and potential inaccuracies in the identification of the region in the second phosphorescence image corresponding to the original tagged region in the first image. The selection of the interrogation windows for lifetime-based MTT image processing often involves a balanced choice between the spatial resolutions of the measurements versus the accuracy of the temperature measurements.

It should be noted that the lifetime-based MTT used in the present study is a Lagrangian method, which is fundamentally different from the LIF-based thermometry approaches of Lu and Melton (2000) and Wolff et al. (2007). The tracer molecules that are tagged by a pulsed laser excitation are imaged at two successive times after the same excitation laser pulse. The accuracy of temperature measurements by using lifetime-based MTT technique is affected by two primary factors: (a) the image noise in the two phosphorescence images leading to noise in the estimated lifetime and (b) potential inaccuracies in the identification of the region in the second phosphorescence image corresponding to the original tagged region in the first image.

The accuracy in the determination of lifetime from Eq. (2), and the resulting accuracy in temperature measurements, is directly influenced by noise in the two phosphorescence signals S_1 and S_2. Even though a 12-bit camera is used in the present study, the actual image noise at each pixel, characterized by the standard deviation of the signal, is found to be in the 3% range. This noise level is connected to the Charge-Coupled Device (CCD) depth of well and the intensifier stage of the CCD. As suggested by Ballew and Demas (1999), the accuracy in calculating the phosphorescence lifetime can be estimated by:

$$\frac{\sigma_\tau}{\tau} = \frac{1}{\ln(S_1/S_2)}\sqrt{\left(\frac{\sigma_{S_1}}{S_1}\right)^2 + \left(\frac{\sigma_{S_2}}{S_2}\right)^2} \tag{3}$$

where σ_{S_1}, σ_{S_2}, and σ_τ are the standard deviations of S_1, S_2, and τ, respectively. The aforementioned 3% phosphorescence signal accuracy at each pixel will, therefore, result in lifetime measurement accuray of about 6% and an instantaneous temperature error of

1.6 °C (using the averaged lifetime temperature sensitivity of 3.6% per degree Celsius for reference). Since this error is unbiased, it can be substantially reduced by averaging over neighboring pixels. Assuming statistical independence, the error can be reduced by the factor $1/\sqrt{N}$, where N is the number of the pixels in the interrogation window. For the results given in the present study based on 21×21 pixel interrogation windows (~20 μm × 20 μm in space), the instantaneous measurement error due to the noise in the acquired phosphorescence images is estimated to be less than 0.3 °C.

In the lifetime-based MTT measurement, the long-lived laser-induced phosphorescence is imaged at two successive times after the same laser excitation pulse. The molecular region tagged in the first image would convect to a new region in the second image according to its Lagrangian displacement over the time delay between the two phosphorescence image acquisitions. To determine the phosphorescence lifetime correctly, this new region in the second phosphorescence image needs to be identified. In the original work of Hu and Koochesfahani (2003, 2006) in developing Molecular Tagging Velocimetry and Thermometry (MTV&T) technique, the new region in the second phosphorescence image corresponding to a tagged molecular region (i.e., interrogation window) in the first phosphorescence image was determined based on a cross-correlation procedure (Gendrich et al., 1997), which determines the displacement vector of the tagged molecular region over the time interval between the two phosphorescence image acquisitions. The procedure is named Molecular Tagging Velocimetry (Koochesfahani and Nocera, 2007), which can be considered as the molecular version of PIV technique.

In present study, the Marangoni flow velocity within convectively-cooled water droplets was measured by using a microscopic Particle Image Velocimetry system. Detailed information about the experimental setup and the micro-PIV measurements is available in Jin (2008). It was found that the Marangoni flow velocity within the convectively-cooled water droplets is on the order of 10 μm/s. Therefore, the displacement of the tagged molecules due to the Marangoni flow during the time delay between the two phosphorescence image acquisitions for the lifetime-based MTT measurements is estimated to be about 0.02 pixels for the present study. The diffusion of the tagged tracer molecules over the time delay between the two phosphorescence image acquisitions may also result in the mismatch of the tagged tracer molecules in the two phosphorescence images. It may affect the accuracy and spatial resolution of the lifetime-based MTT measurements. According to Miles et al. (2000), the displacement of the tagged molecules due to the molecular diffusion over the time delay between the two phosphorescence image acquisitions can be estimated to be less than 0.2 pixels for the present study. In the present study, interrogation windows of 21×21 pixels (about 20 μm × 20 μm in space) were used for the lifetime-based MTT image processing. The interrogation windows were chosen at the same locations for the first and second phosphorescence images. In order to assess the uncertainty level in the final measured temperature by ignoring the effects of the Marangoni flow velocity and molecular diffusion, temperature field was computed using regions in the second phosphorescence image that were deliberately displaced an additional ±1 pixel to exaggerate the effects of the convective Marangoni velocity and molecular diffusion. The "induced" mismatch resulted in a temperature error of about 0.2 °C for the conditions of the present study. In addition, the procedure described here was also applied to the case of a water droplet at room temperature, for which the temperature distribution within the water droplet should be uniform and constant. The measured temperature distribution within the droplet was found to have an uncertainty within 0.5 °C, which is the total measurement uncertainty and accounts for all the effects discussed above.

It should also be noted that, although the laser-sheet thickness (~200 μm) is significant relative to the drop radius (~400 μm), the depth of field of the microscopic objective used in the present study is only about 3.5 μm. The situation is similar to the measurements by using microscopic PIV technique (Olsen and Adrian, 2000; Meinhart et al., 2000; Bourdon et al., 2004) and microscopic LIF technique (Natrajan and Christensen, 2009; Motosuke et al., 2009; Ichiyanagi et al., 2009) in micro-flows with volume illumination. According to Olsen and Adrian (2000) and Meinhart et al. (2000), the flux of the photoluminescence light from an excited particle/molecule that reaches the image plane (i.e., the photoluminescence intensity collected by the image detector through microscopic objective) would decrease significantly as the particle/molecule is away from the focal plane of the microscopic objective. Based on the theoretic equation given in Olsen and Adrian (2000), the detected phosphorescence intensity of the tagged tracer molecules at 7.0 μm away from the focal plane of the microscopic objective (i.e., twice of the depth of field of the microscopic objective used in the present study) was estimated to become less than 8.0% of the intensity from the same amount of tagged tracer molecules in the focal plane of the microscopic objective for the present study. Therefore, the spatial resolution of the MTT measurements in the direction normal to the microscopic objective's focal plane is mainly determined by the depth of field of the microscopic objective rather than the laser-sheet thickness. However, it should be noted that, although their contributions become much less importance, the excited unfocused tracer molecules, which lie outside the focal plane of the microscopic objective, would also be detected as the background intensities in the acquired phosphorescence images. Further investigation is planned to quantify the effects of the background intensities from the unfocused tracer molecules on the temperature measurements.

5. Measurement results and discussions

Fig. 5 shows a typical pair of acquired phosphorescence images for MTT measurements and the instantaneous temperature distribution inside the water droplet derived from the phosphorescence image pair. The image pair was taken at 5.0 s later after the water droplet (initial temperature 20.5 °C) impinged onto the cold test plate (T_w = 5.0 °C). As described above, the first image (Fig. 5a) was acquired at 0.5 ms after the laser excitation pulse and the second image (Fig. 5b) at 3.5 ms after the same laser pulse with the same exposure time of 1.5 ms for the two image acquisitions. Since the time delays between the laser excitation pulse and the phosphorescence image acquisitions can eliminate scattered/reflected light and any fluorescence from other substances (such as from the surface of the test plate) in the measurement region effectively, the phosphorescence images of the water droplet are quite "clean" even though no optical filter was used in the present study for the phosphorescence image acquisition.

As described above, Eq. (2) can be used to calculate the phosphorescence lifetime of the tagged molecules on a pixel-by-pixel basis, which results in a distribution of the phosphorescence lifetime over a two-dimensional domain. With the calibration profile of phosphorescence lifetime versus temperature as shown in Fig. 2, a two-dimensional, instantaneous temperature distribution within the water droplet can be derived from the phosphorescence image pair. As described above, interrogation windows of 21×21 pixels (~20 μm × 20 μm in space) were used in the present study for the lifetime-based MTT image processing to balance the spatial resolution of the measurements versus the accuracy of the temperature measurements. Fig. 5c shows the instantaneous temperature distribution derived from the phosphorescence image pair with interrogation windows of 21×21 pixels (~20μm × 20 μm in

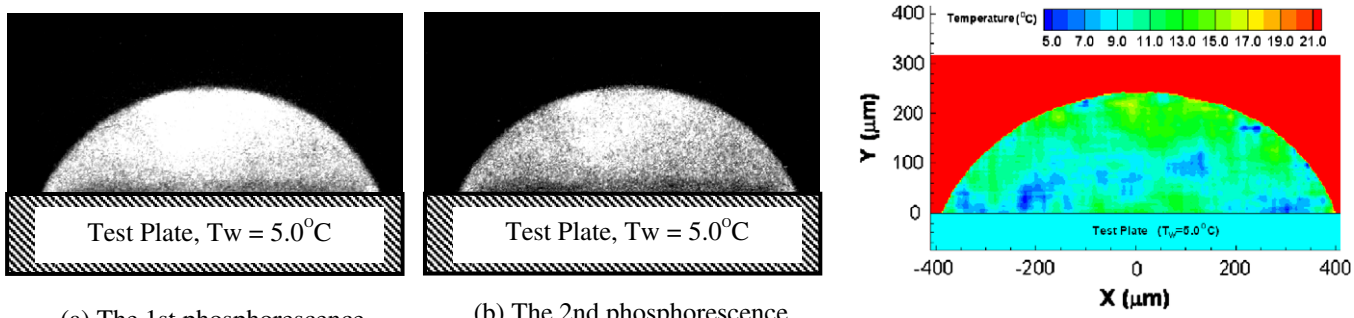

(a) The 1st phosphorescence image acquired at 0.5 ms after the laser pulse

(b) The 2nd phosphorescence image acquired at 3.5 ms after the same laser pulse

(c) Corresponding MTT result derived from the image pair

Fig. 5. A typical MTT measurement when the surface temperature of the test plate was set to $T_W = 5.0$ °C.

space). Based on a time sequence of the measured transient temperature distributions within the water droplet as the one shown in Fig. 5c, the unsteady heat transfer process within the convectively-cooled water droplets was revealed quantitatively.

Fig. 6 shows the spatially-averaged temperature of the water droplet as a function of the time after it impinged onto the cold test plate, which was calculated based on the time sequence of instantaneous MTT temperature distributions. The characteristics of the unsteady heat transfer within the water droplet in the course of convectively cooling process were revealed quantitatively from the time evolution of the spatially-averaged temperature of the water droplet. Since initial temperature of the water droplet (20.5 °C) was significantly higher than that of the cold test plate ($T_W = 5.0$ °C), the temperature of the water droplet was found to decrease rapidly after it impinged on the test plate. The measurement results given in Fig. 6 also revealed that a thermal steady state would be reached at about 20 s after the water droplet impinged on the cold test plate. The spatially-averaged temperature of the water droplet would not decrease anymore when the thermal steady state was reached.

When the temperature of the test plate was set below the freezing temperature, water droplets impinging on the test plate were found to turn to ice rapidly. It should be noted that one of the technical challenges to achieve quantitative temperature measurements within icing water droplets is the expulsion of the tracer molecules from the liquid water during the icing process (much like salt is expelled from a saline solution during freezing). This would concentrate the tracer molecules in the remaining liquid and cause significant errors in the temperature measurements

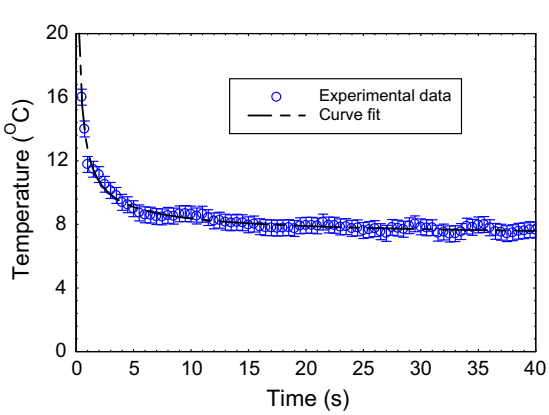

Fig. 6. Spatially-averaged temperature of the water droplet versus time when the surface temperature of the test plate was set to $T_W = 5.0$ °C.

for commonly-used LIF-based thermometry techniques. As described above, since the lifetime-based MTT technique used in the present study is a ratiometric approach, it can eliminate the effects of the concentration variations due to the expulsion of phosphorescent tracer molecules during freezing process on temperature measurements effectively.

Fig. 7 shows the time sequence of the acquired phosphorescence images of a water droplet when it impinged onto the frozen cold test plate ($T_W = -2.0°C$). The corresponding instantaneous temperature distributions of the remaining liquid water within the icing droplet measured by using the lifetime-based MTT technique are given in Fig. 8. The transient behavior of the phase changing process within the small icing water droplet was revealed clearly from the acquired phosphorescence images and the MTT measurement results. In the phosphorescence images, the "brighter" region (i.e., more concentrated dye due to the expulsion of the phosphorescence tracer molecules during icing process) in the upper portion of the droplet represents liquid phase – water; while the "darker" region at the bottom indicates solid phase – ice. It can be seen clearly that the liquid water at the bottom of the droplet was frozen and turned to solid ice rapidly since the wall temperature of the test plate was below frozen temperature, while the upper portion of the droplet was still in liquid state. As the time goes by, the interface between the liquid phase water and solid phase ice was found to move upward continuously. As a result, the droplet was found to grow upward with more and more liquid phase water turning to solid phase ice. At about 35 s after the droplet impinged onto the cold test plate, the droplet was found to turn completely into a solid ice crystal completely.

It should be noted that, as shown clearly in the acquired phosphorescence image given in Fig. 7f, a distinctive cusp-like tip is found to protrude from the top surface of the droplet when the water droplet was frozen completely to become an ice crystal. The formation of distinctive cusp-like tips on the top frozen droplets was also observed for all the other test cases with different surface temperatures of the frozen cold test plate. The observations indicate that a frozen droplet would have cusp-like sharp tip instead of a round top. A similar cusp-like shape top was also reported by Anderson et al. (1996) when they studied droplet solidification process for ultrapure material production. They also suggested that a theory involving dynamics growth angles at the tri-junction between solid ice, liquid water, and surrounding air can be used to explain the formation of the cusp-like sharp top in droplet solidification process.

Based on the time sequences of the instantaneous MTT measurements results as those shown in Fig. 8, the time evolution of the averaged temperature of the remaining liquid water within the icing droplet in the course of icing process were calculated,

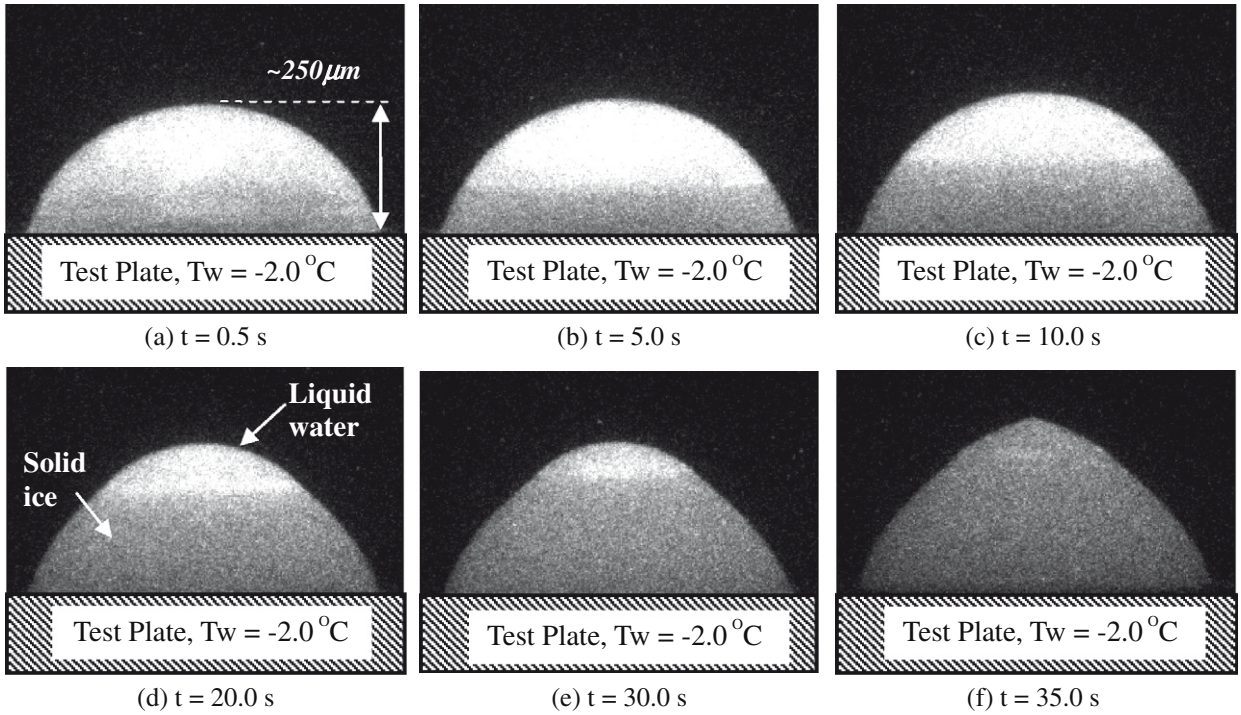

(a) t = 0.5 s (b) t = 5.0 s (c) t = 10.0 s

(d) t = 20.0 s (e) t = 30.0 s (f) t = 35.0 s

Fig. 7. Time sequence of the acquired phosphorescence images to visualize the icing process (the surface temperature of the test plate was set to $T_W = -2.0$ °C).

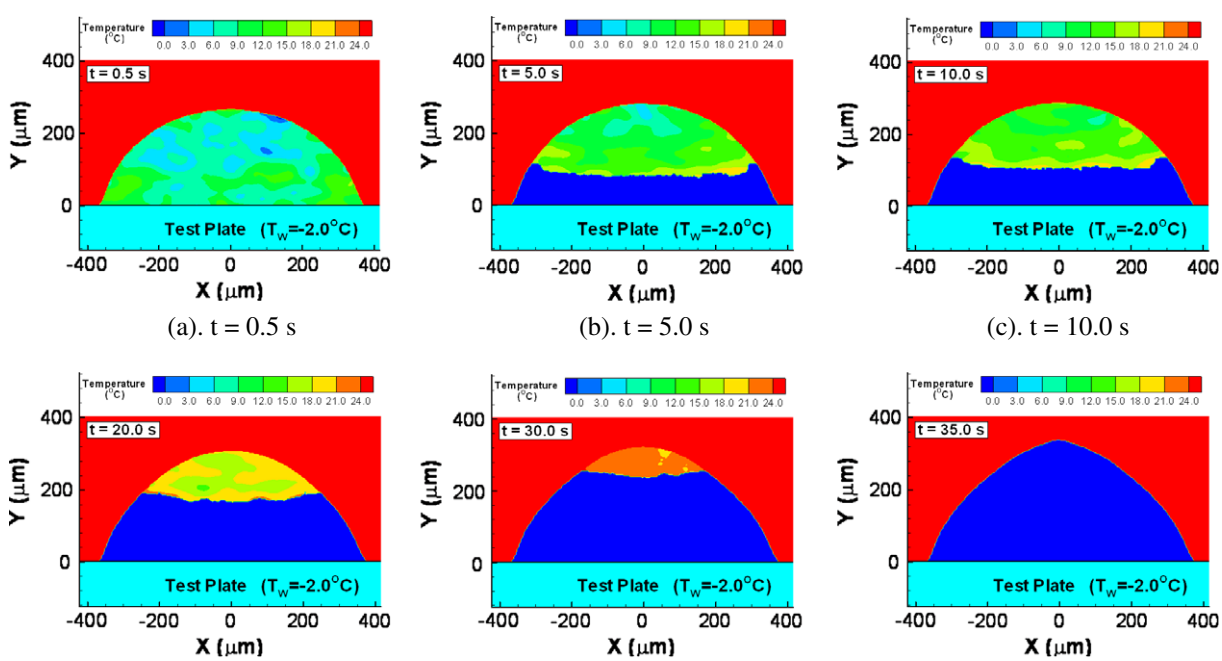

(a). t = 0.5 s (b). t = 5.0 s (c). t = 10.0 s

(d). t = 20.0 s (e). t = 30.0 s (f). t = 35.0 s

Fig. 8. Corresponding MTT measurements in the course of icing process with the surface temperature of the test plate set to $T_W = -2.0$ °C.

which is shown in Fig. 9. As described above, the initial temperature of the liquid water droplet was 20.5 °C before impinging onto the frozen cold test plate. The temperature of the water droplet is expected to decrease with the time after it impinged onto the cold test plate, as the one shown in Fig. 6, if the temperature of the cold test plate is above freezing (i.e., there is not phase changing process involved). Surprisingly, the measurement results given in Fig. 9 reveal a completely different trend data for the icing droplet. The averaged temperature of the remaining liquid water within the icing droplet was found to increase monotonically with time in the course of icing process. It should be noted that, since the frame rate for the phosphorescence image acquisition used in the present study is relative low, (i.e., $f = 2$ Hz), the details of the initial temperature drop of the water droplet at the moment as it impinged onto the frozen cold test plate were not able to be resolved due to the limited temporal resolution of the present measurements.

The unexpected temperature increase of the remaining liquid water within the droplet in the course of the icing process is

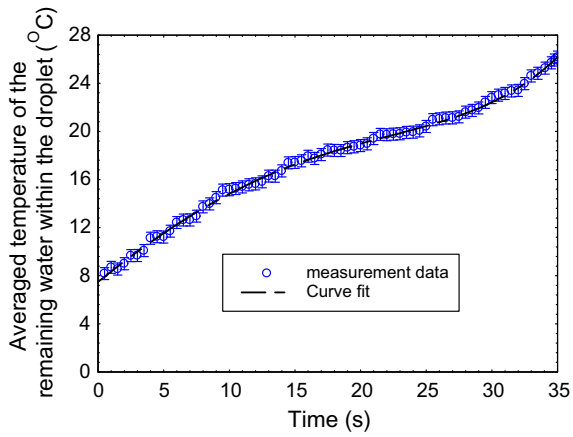

Fig. 9. The averaged temperature of the remaining liquid water in the icing droplet versus time when the surface temperature of the test plate was set to $T_W = -2.0$ °C.

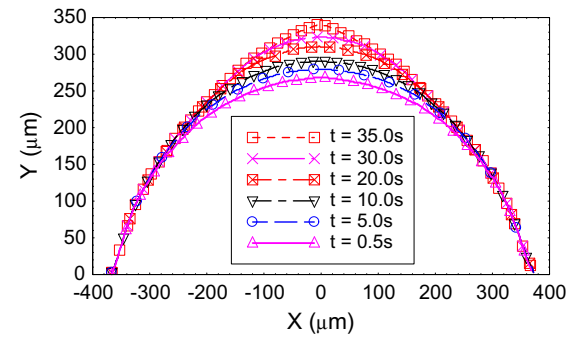

Fig. 10. The variations of the shape profile the icing droplet versus time when the surface temperature of the test plate was set to $T_W = -2.0$ °C.

believed to be closely related to the heat release of the latent heat of solidification. As visualized clearly from the MTT measurement results given in Fig. 8, the liquid water at the bottom of the icing droplet would turn to solid ice rapidly after the droplet impinged onto the frozen cold test plate. It is well known that there will be a significant amount of latent heat of solidification being released as liquid water turned to solid ice. According to the physics textbook of Cutnell and Johnson (1995), the specific latent heat of solidification for water is 334 kJ/kg (i.e., 79.7 cal/g). While some of the released latent heat of solidification would be conducted through the cold test plate and dissipated by the thermal bath circulator, a portion of the released latent heat of solidification would be conducted through the interface between the solid ice and the liquid water within the icing droplet to heat the remaining liquid water with the icing droplet. In the course of icing process, more and more liquid water was found to turn to ice with the latent heat of solidification releasing continuously, while the total amount of the remaining liquid water within the icing droplet would become less and less. As a result, the averaged temperature of the remaining liquid water within the icing droplet would increase monotonically with time until the droplet turned to ice crystal completely, which is at about 35 s after it impinged onto the frozen cold test plate for the case shown in Fig. 8. It should be noted that, the rapid temperature rise during the freezing of liquid metals caused by the release of latent heat as the metals undergo a change in crystalline structure is actually well known in material science and engineering community; these are usually called "*recalescence*" phenomena (Hofmeister et al., 1990).

Based on the acquired phosphorescent images, the shape profile of the icing droplet in the course of icing process can also be extracted, which is given in Fig. 10. The time evolution of the droplet shape profile in the course of the icing process was revealed quantitatively. It can be seen clearly that the water droplet was round, as a cap of a sphere, at the beginning, as expected. As visualized clearly in the acquired phosphorescence images and MTT measurements described above, the liquid water at the bottom of the droplet would be frozen and turned to solid ice rapidly, while the upper portion of the droplet was still in liquid state. As the time goes by, the droplet would grow upward with more and more liquid water turned to solid ice within the icing droplet. As a result, the rounded, spherical-cap-shaped profile of the droplet was found to be sharpened substantially at the top to become a prolate-spheroid-shaped profile. Eventually, the rounded, spherical-cap-shaped water droplet was found to turn to a prolate-spheroid-shaped ice crystal with distinctive cusp-like top at the end of the icing process.

It is well known that a liquid water droplet will experience volume expansion as it is turning into solid ice. The time evolution of the droplet volume expansion in the course of the icing process was also revealed clearly and quantitatively from the variation of the droplet shape profiles given in Fig. 10. It can be seen clearly that, while the contact radius of the droplet on the test plate is almost constant, the height of the droplet was found to increase continuously during the icing process. It indicates that, in the course of icing process, the volume expansion of the water droplet would be mainly upward to cause droplet growth in height rather than in radius. As described above, the laser illuminating plane is along the middle plane of the droplet for the present MTT measurements, the volume of the droplet can be determined based on the droplet shape profiles with a reasonable assumption of the droplet being axisymmetric. Fig. 11 shows the time histogram of the volume expansion of the droplet, V/V_O, in the course of the icing process, where V_O is the initial volume of the water droplet. It can be seen clearly that the volume of the droplet was found to increase rapidly at the beginning of the icing process since the majority of the droplet was still in liquid water state. The volume expansion rate was found to decrease with time since less and less liquid water was found to remain within the droplet. The volume expansion profile was found to become a flat line at about 35 s after the droplet impinged onto the frozen cold test plate, which indicates that the volume of the droplet would not change with time anymore after the water droplet turned to solid ice crystal completely.

The time variation of the averaged specific weight (thereby density) of the droplet, γ, in the course of the icing process can also be determined based on the measured droplet volume expansion profile, which is also given in Fig. 11. For comparison, the standard

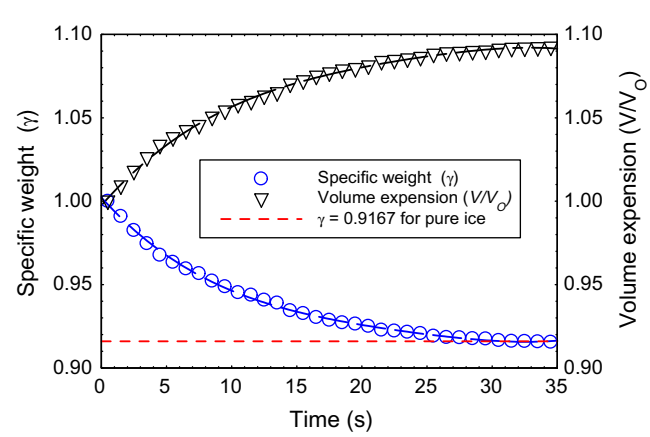

Fig. 11. The volume (V/V_O) and the specific weight (γ) of the icing droplet versus time when the surface temperature of the test plate was set to $T_W = -2.0$ °C.

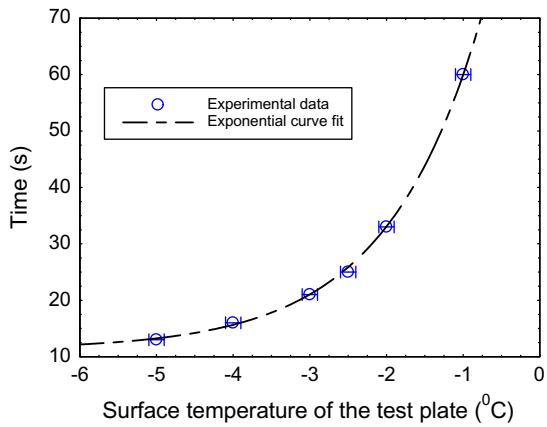

Fig. 12. The required freezing time versus the test plate temperature.

value of the specific weight of pure ice (i.e., γ_{ice} = 0.9168) was also given in the figure as the dashed straight line. It can be seen clearly that the specific weight (or density) of the droplet was found to become smaller and smaller as more and more remaining liquid water within the droplet turned to solid ice. As it is expected, the profile of the measured specific weight of the icing droplet was found to approach the standard value of the specific weight of ice (i.e., γ_{ice} = 0.9168) as the time goes by. When the water droplet turned to solid ice crystal completely at 35 s after it impinged onto the frozen cold test plate, the measured value of the specific weight of the ice crystal was found to be γ = 0.9165, which agree with the standard value of specific weight of pure ice γ_{ice} = 0.9168 very well.

The required freezing time, which is defined as the time interval between the moment when a water droplet impinged on the frozen cold test plate and the moment when the water droplet was found to turn to an ice crystal completely, can also be determined based on the time sequences of the MTT measurements as those reported above. The information about the required freezing time is of great important to wind turbine icing phenomena since the required frozen time would determine the types of the ice formation on wind turbine blades being rime ice or glaze ice (Fortin and Perron, 2009). Fig. 12 shows the variations of the required freezing time of the water droplets with the surface temperature of the freezing cold test plate changed from −1.0 °C to −5.0 °C. As it is expected, the required freezing time for the water droplets (initial temperature at 20.5 °C) turned to ice crystal was found to strongly depend on the surface temperature of the test plate. An exponential curve was found to fit the measurement data very well to represent the relationship between the required freezing time and the surface temperature of the frozen cold test plate.

6. Conclusions

An experimental investigation was conducted to quantify the unsteady heat transfer and phase changing process within small icing water droplets in order to elucidate underlying physics to improve our understanding of the important micro-physical process pertinent to wind turbine icing phenomena. A lifetime-based molecular tagging thermometry (MTT) technique was developed and implemented to reveal the time evolution of the unsteady heat transfer and dynamic phase changing process within small icing water droplets in the course of icing process, which is pertinent to the ice formation and accretion process as water droplets impinging onto frozen cold wind turbine blades. For the lifetime-based MTT measurements, a pulsed laser is used to "tag" phosphorescent molecules premixed within the small water droplets. Long-lived laser-induced phosphorescence is imaged at two successive times after the same laser excitation pulse. The temperature measurement is achieved by taking advantage of the temperature dependence of phosphorescence lifetime, which is estimated from the intensity ratio of the acquired phosphorescence image pair.

The time evolution of the unsteady heat transfer and phase changing process within small icing water droplets was revealed clearly and quantitatively based on the MTT measurements. It was found that, after water droplet impinged onto the frozen cold test plate, the liquid water at the bottom of the droplet was found to be frozen and turned to solid ice rapidly, while the upper portion of the droplet was still in liquid state. As the time goes by, the interface between the liquid phase water and solid phase ice was found to move upward continuously with more and more remaining liquid water within the droplet turned to solid ice. The round, spherical-cap-shaped profile of the water droplet was found to be sharpened continuously to become a prolate-spheroid-shaped profile. A cusp-like sharp tip instead of a round top was found to protrude at the top of the droplet at the end of the icing process. Interestingly, the averaged temperature of the remaining liquid water within the icing droplet was found to increase rather than decrease monotonically in the course of icing process. The temperature increase of the remaining water with the icing droplet is believed to be caused by the significant heat release of the latent heat of solidification during the icing process. As it is expected, while the volume of the droplet was found to increase with time monotonically, the specific weight (thereby the density) of the icing droplet would decrease with time monotonically in the course of icing process, approaching the standard value of pure ice as the droplet turned to ice crystal completely. The volume expansion of the water droplet was found to be mainly upward to cause droplet height growth rather than radial to enlarge the contact area of the droplet on the test plate in the course of the icing process. The required frozen time of the droplet was found to strongly depend on the temperature of the test plate, which would decrease exponentially with the decreasing surface temperature of the frozen cold test plate. The new findings derived from the icing physics studies as the one reported at here would lead to a better understanding of the important micro-physical processes, which could be used to improve current icing accretion models for more accurate prediction of ice formation and ice accretion on wind turbine blades as well as development of effective anti-/de-icing strategies tailored for safer and more efficient operation of wind turbines in cold weather.

Acknowledgments

The authors want to thank Dr. M.M. Koochesfahani of Michigan State University for providing chemicals used for the present study. The support of National Science Foundation CAREER program under award number of CTS-0545918 is gratefully acknowledged.

References

Anderson, D.M., Worster, M.G., Davis, S.H., 1996. The case for a dynamic contact angle in containerless solidification. J. Cryst. Growth 163, 329–338.
Ballew, R.M., Demas, J.N., 1999. An error analysis of the rapid lifetime determination method for the evaluation of single exponential decay. Anal. Chem. 61, 30–33.
Bourdon, C.J., Olsen, M.G., Gorby, A.D., 2004. Validation of an analytical solution for depth of correlation in microscopic particle image velocimetry. Meas. Sci. Technol. 15, 318–327.
Coppeta, J., Rogers, C., 1998. Dual emission laser induced fluorescence for direct planar scalar behavior measurements. Exp. Fluids 25, 1–15.
Cutnell, J.D., Johnson, K.W., 1995. Physics, third ed. Wiley, New York.
Dalili, N., Edrisy, A., Carriveau, R., 2009. A review of surface engineering issues critical to wind turbine performance. Renew. Sust. Energy Rev. 13, 428–438.
Ferraudi, G.J., 1988. Elements of Inorganic Photochemistry. Wiley-Interscience, New York.
Fortin, G., Perron, J., 2009. Wind turbine icing and de-icing. AIAA-2009-274, 47th AIAA Aerospace Sciences Meeting including the New horizons Forum and Aerospace Exposition, Orland, Florida, 5–8 January, 2009.

Gendrich, C.P., Koochesfahani, M.M., Nocera, D.G., 1997. Molecular tagging velocimetry and other novel applications of a new phosphorescent supramolecule. Exp. Fluids 23 (5), 361–372.
Hansman Jr., R.J., Turnock, S.R., 1989. Investigation of surface water behavior during glaze ice accretion. J Aircraft 26 (2), 140–147.
Hartmann, W.K., Gray, M.H.B., Ponce, A., Nocera, D.G., 1996. Substrate induced phosphorescence from cyclodextrin–lumophore host-guest complex. Inorg. Chim. Acta. 243, 239–248.
Harris, S.R., Lempert, W.R., Hersh, L., Burcham, C.L., Saville, D.A., Miles, R.B., Gee, K., Haughland, R.P., 1996. Quantitative measurements of internal circulation in droplets using flow tagging velocimetry. AIAA J. 34 (3), 449–454. doi:10.2514/3.13088.
Hochart, C., Fortin, G., Perron, J., 2008. Wind turbine performance under icing conditions. Wind Energy J. 11, 319–333.
Homola, M.C., Nicklasson, P.J., Sandsbo, P.A., 2006. Ice sensors for wind turbines. Cold Reg. Sci. Technol. 46, 125–131.
Hofmeister, W.H., Bayuzick, R.J., Robinson, M.B., 1990. Dual purpose pyrometer for temperature and solidification velocity-measurement. Rev. Sci. Instrum. 61, 2220–2223.
Hu, H., Koochesfahani, M.M., 2003. A novel technique for quantitative temperature mapping in liquid by measuring the lifetime of laser induced phosphorescence. J. Visualization 6, 143–153.
Hu, H., Koochesfahani, M.M., 2006. Molecular tagging velocimetry and thermometry and its application to the wake of a heated circular cylinder. Meas. Sci. Technol. 17, 1269–1281.
Hu, H., Lum, C., Koochesfahani, M.M., 2006. Molecular tagging thermometry with adjustable temperature sensitivity. Exp. Fluids 40, 753–763.
Hu, H., Huang, D., 2009. Simultaneous measurements of droplet size and transient temperature within surface water droplets. AIAA J. 47 (4), 813–820.
Ichiyanagi, M., Sasaki, S., Sato, Y., Hishida, K., 2009. Micro-PIV/LIF measurements on electrokinetically-driven flow in surfacemodified microchannels. J. Micromech. Microeng. 19, 045021.
Jasinski, W.J., Noe, S.C., Selig, M.C., Bragg, M.B., 1998. Wind turbine performance under icing conditions. Trans. ASME J. Sol. Energy Eng. 120, 60–65.
Jin, Z., 2008. Experimental investigations of micro-scale thermal flow phenomena by using advanced flow diagnostic techniques. Ph.D. Thesis, Department of Aerospace Engineering, Iowa State University, December 2008.
Koochesfahani, M.M., Nocera, D.G., 2007. Molecular tagging velocimetry. In: Foss, J., Tropea, C., Yarin, A. (Eds.), Handbook of Experimental Fluid Dynamics. Springer-Verlag (Chapter 5.4).
Laakso, T., Peltola, E., 2005. Review on blade heating technology and future prospects. In: BOREAS VII Conference, 7–8th March 2005. Saarislkä, Finland.
Lu, Qand.A., Melton, A., 2000. Measurement of transient temperature field within a falling droplet. AIAA J. 38, 95–101.
Meinhart, C.D., Wereley, S.T., Gary, M.H.B., 2000. Volume illumination for two-dimensional particle image velocimetry. Meas. Sci. Technol. 11, 809–814.
Miles, R.B., Grinstead, J., Kohl, R.H., Diskin, G., 2000. The RELIEF flow tagging technique and its application in engine testing facilities and for helium-air mixing studies. Meas. Sci. Technol. 11 (9), 272–1281. doi:10.1088/0957-0233/11/9/304.
Motosuke, M., Akutsu, D., Honami, S., 2009. Temperature measurement of microfluids with high temporal resolution by laser-induced fluorescence. J. Mech. Sci. Technol. 23, 1821–1828.
Natrajan, V.K., Christensen, K.T., 2009. Two-color laser-induced fluorescent thermometry for microfluidic systems. Meas. Sci. Technol. 20, 015401.
Olsen, M.G., Adrian, R.J., 2000. Out-of-focus effects on Particle image visibility and correction in microscopic particle image velocimetry. Exp. Fluids s166, 194.
Omrane, A., Juhlin, G., Ossler, F., Aldén, M., 2004a. Temperature measurements of single droplets by use of laser-induced phosphorescence. Appl. Optics 43, 3523–3529.
Omrane, A., Santesson, S., Aldén, M., Nilsson, S., 2004b. Laser techniques in acoustically levitated micro droplets. Lab-on-a-Chip 4, 287–291.
Pringsheim, P., 1949. Fluorescence and Phosphorescence. Interscience, New York.
Seifert, H., Westerhellweg, A., Kröning, L., 2003. Risk analysis of ice thrown from wind turbines. In: BOREAS VI Conference, April, 2003. Pyhä, Finland.
Tammelin, B., Cavaliere, M., Holttinen, H, Morgan, C, Seifert, H, Santti, K., 1998. Wind energy production in cold climate (WECO). Publishable report 1–38.
Wolff, M., Delconte, A., Schmidt, F., Gucher, P., Lemoine, F., 2007. High-pressure diesel spray temperature measurements using two-color laser induced fluorescence. Meas. Sci. Technol. 18, 697–706.